# Interplay of nuclear structure and dynamics with light exotic beams: the study of the reactions $^{8}$B+$^{64}$Zn and $^{9}$Li-$^{4}$He

*Alessia* Di Pietro[1,*], *Roberta* Spartá[1,2], *Juan Pablo* Fernandez Garcìa[3], *Pierpaolo* Figuera[1], *Marco* La Cognata[1], *Antonio M* Moro[3], *Alan C* Shotter[4], and *Domenico* Torresi[1]

[1]INFN, Laboratori Nazionali del Sud, via S. Sofia 62, 1-95123 Catania, Italy
[2]Facoltà di Ingegneria, Università Kore, 94100 Enna, Italia.
[3]Departamento de FAMN, Universidad de Sevilla, Apartado 1065, 41080 Sevilla, Spain
[4]School of Physics and Astronomy, University of Edinburgh, JCMB, Peter Guthrie Tait Road, EH9 3FD, Edinburgh, UK

**Abstract.** This paper reports on investigations of elastic scattering reactions involving both, one proton-rich and one neutron-rich radioactive nuclei, $^{8}$B and $^{9}$Li respectively. These investigations highlighted the effects that the peculiar nuclear structure of these nuclei has on the reaction dynamics.

## 1 Introduction

It is well assessed that in the elastic scattering of neutron-halo projectiles with well bound targets, coupling to the continuum results in a suppression in the elastic scattering cross section (e.g. [1–5]) ensuing a large total reaction cross-section. A large fraction of the total reaction cross-section is due to processes like break-up or transfer [2, 6, 7]. The elastic scattering of the proton-halo $^{8}$B nucleus on a $^{64}$Zn target is compared with the scattering by neutron-halo nuclei on the same target. $^{8}$B with its very low breakup threshold ($S_p$=138 keV) has a proton-halo structure. At variance with the neutron-halo case, due to the additional Coulomb interaction of the proton in the halo with both, the core and the target, the dynamics of proton-halo is expected to be different than neutron-halo.
Previous experiments with the proton-halo $^{8}$B, used an in-flight produced beam which had limitations in terms of beam purity, energy spread and beam emittance [8, 9]. They found that the total reaction cross-section was as large as neutron-halo reactions. The availability at HIE-ISOLDE of a post accelerated $^{8}$B beam gave the possibility to investigate the reaction dynamics of this proton-halo nucleus with a much better precision leading to a different conclusion than in previous experiments.

This manuscript reports also on the measurement of the elastic scattering excitation function of the neutron-rich $^{9}$Li nucleus on a $^{4}$He target. Antisymetrised-Molecular-Dymanics calculations [10] show that the reaction $^{9}$Li+$^{4}$He can be influenced by a rotational band structure of the compound nucleus $^{13}$B of Li-He type. Such a rotational band would produce resonances in the $^{9}$Li+$^{4}$He elastic channel excitation function. On the other hand, the presence of resonances in the excitation function may not be necessarily associated to compound nucleus states but rather to dynamic effects. These effects may be originated by the extended surface of neutron rich nuclei. In fact, possible transient molecular systems can be formed between the $^{9}$Li and $^{4}$He ions. For some given impact parameter the $^{4}$He can be temporarily captured by the weak attraction of the neutron tail of $^{9}$Li and starts to rotate about it. The $^{4}$He can be either emitted back into the entrance channel, or excite inelastic degrees of freedom leading to other reaction channels. As a consequence the elastic excitation function may show broad resonances. The nature of such broad resonances has been investigated using an orbiting scenario. The results of this investigation are reported in the present contribution.

## 2 The $^{8}$B+$^{64}$Zn reaction

The reaction $^{8}$B+$^{64}$Zn was measured at HIE-ISOLDE at CERN with the ISOL $^{8}$B beam [11]. The $^{8}$B beam was accelerated to an energy of 4.9×A MeV and had an average intensity on target of ∼400pps. The reaction target was 1.021 mg/cm$^2$ isotopically enriched $^{64}$Zn; it was angled at 30° with respect to the beam axis to allow measurements at 90°. The experimental setup consisted of six silicon telescopes made of two stages of detectors, 40 $\mu$m and 1000 $\mu$m thick respectively. Each detector was a 50x50 mm$^2$ Doube Sided Silicon Strip Detector (DSSSD) segmented into 16+16 strips [12]. Thanks to the high segmentation, the angular resolution was limited only by statistics and not by the angular granularity of the set-up.

The $^{8}$B+$^{64}$Zn elastic scattering angular distribution, as ratio to Rutherford, is shown in fig. 1. Unlike the neutron-halo nucleus $^{11}$Be at similar $E_{\mathrm{c.m.}}/V_{\mathrm{C}}$ [4, 5], a clear Coulomb-nuclear interference peak is visible at around 35°. The elastic cross section was compared with continuum-discretized coupled-channels (CDCC) calcula-

*e-mail: dipietro@lns.infn.it

tions which are shown in figure 1a as full line. In these calculations the $^8$B is described as a two-cluster system, a $^7$Be and a proton [11]. Also shown as dashed line in figure 1a, calculations where the coupling to the continuum was not considered.

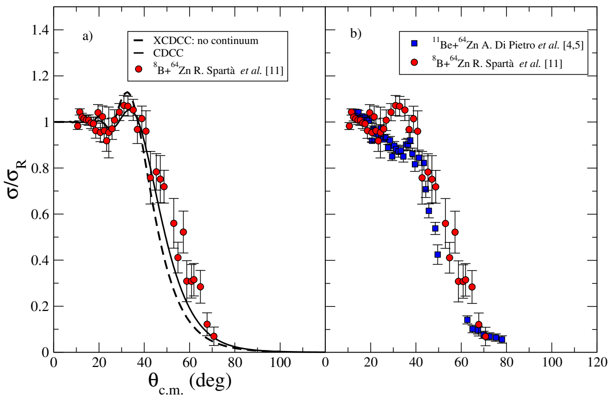


**Figure 1.** a) Elastic scattering angular distribution for $^8$B+$^{64}$Zn (symbols). CDCC calculations with (full line) and without (dashed line) coupling to the continuum. b) Elastic scattering angular distribution, as ratio to Rutherford, of $^8$B+$^{64}$Zn (red circles) and $^{11}$Be+$^{64}$Zn (blue squares). The data of $^{11}$Be+$^{64}$Zn are from [4, 5].

CDCC calculations are in agreement with the experimental data. From the comparison of the calculations with and without coupling to the continuum, emerges that, contrary to what happens in the neutron-halo case, this coupling produces only a small suppression of the elastic cross-section in the Coulomb-nuclear interference region. The total reaction cross-section deduced from the CDCC calculations, $\sigma_R$ =1.5 b, is much smaller than what obtained with the neutron-halo $^{11}$Be ($\sigma_R$=2.7 b) on the same target and at similar $E_{c.m.}/V_C$ [4, 5]. This result appears to be at variance with what reported in [9, 13], where a total reaction cross-section in agreement with the systematics for the neutron-halo systems has been reported.
The comparison of the experimental elastic scattering angular distribution, one involving the neutron-halo $^{11}$Be (squares) [4, 5] and the other involving the proton-halo $^8$B (circles), at similar $E_{c.m.}/V_C$ on the same $^{64}$Zn target, is shown in figure 1b as ratio to Rutherford. From this comparison, one can clearly see that the $^8$B angular distribution differs significantly from that of the neutron-halo $^{11}$Be [4**?** ]. The difference is mainly in the Coulomb-nuclear interference region, indicating that $^8$B does not show the strong effects of long-range absorption observed in the neutron-halo case. The reason for that can be attributed to both, the presence of a Coulomb and of a centrifugal barrier between the proton in the halo and the 7Be core, as studied in [14].

## 3 The $^9$Li+$^4$He experiment

The $^9$Li+$^4$He experiment was performed at TRIUMF (Canada) [15] using the Thick Target Inverse Kinematic (TTIK) technique [16]. A 32 MeV $^9$Li beam is slowed down in a tick $^4$He gas target until it stops before reaching the detector placed at 0°. The recoiling $\alpha$ particles, owing to the lower stopping power than the beam, have sufficient kinetic energy to reach the detectors. The target consisted of the TUDA chamber (a scheme of the set up is shown in [15]) filled with isotopically pure $^4$He gas at pressure of 650 Torr. A Kapton window $\approx$ 12 $\mu$m thick separated the gas-filled chamber from the high vacuum beam line. The detection system consisted of three telescopes each made of 50×50 mm$^2$, 50 $\mu$m thick silicon detector segmented into four-quadrants as ΔE and a 50×50 mm$^2$ and 1500 $\mu$m thick single PAD silicon as residual energy detector. Elastically scattered $\alpha$-particles were detected and discriminated from other reaction processes using Time of Flight (ToF) techniques. The start for the ToF measurement was given by a microchannel plate (MCP) detector placed under vacuum [17]. This produced a signal whenever a $^9$Li beam particle was entering the target. Hence, the MCP detector was also used to count the beam particles for cross-section normalisation. The stop to the ToF was provided by the recoiling $\alpha$ particles reaching the silicon detector. The beam intensity was kept below $10^6$ pps to avoid saturation and/or pileup of the MCP signal.

Monte Carlo simulations were performed to determine the relationship between measured quantities (energies and position of the detected $\alpha$s) and the corresponding c.m. variables. A Monte Carlo code was especially written for performing such simulations. The simulations included energy and angular straggling for the beam and the recoiling $\alpha$-particles. The $^9$Li+$^4$He excitation function was obtained in the $E_{c.m.}$ range 3.5 MeV - 9 MeV. With the TTIK technique, each measured point in the $\frac{d\sigma}{d\Omega}(E_{c.m.})$ corresponds to a $\theta_{c.m.}$ which changes with energy. In fig. 2a is shown the excitation function measured in the detector placed at $\theta_{lab}$ ~0°.

The excitation function represented in figure 2a is caracterised by two broad resonances. The angular distributions measured at backward angles, at energies corresponding to the two resonances, are peaked at $\theta_{c.m.}$ =180° (see fig.2b,c). These backward-peaked broad resonances may be originated from an orbiting-type phenomenon which leads to the formation of a transient quasi-molecular system. This phenomenon is essentially a rolling process where the colliding $^9$Li and $\alpha$ encounter each other at the surface, at an impact parameter near the sum of their radii; after attachment and rolling, they separate. The large width of the resonances reflects the short half-life of the process. The angular distributions of the resonances is characteristic of the relative orbital angular momentum $\ell$ [18]. For neutron rich nuclei, the surface interaction region can be extended. In particular, for the $^9$Li+$^4$He collision, the extended low density neutron field of $^9$Li provides a weak attraction for orbital angular momentum components of the wave function corresponding to peripheral interactions between the two ions. In [15], in order to explain the observed resonances, a model, called Transient Rotational Model (TRM), was developed. To perform the

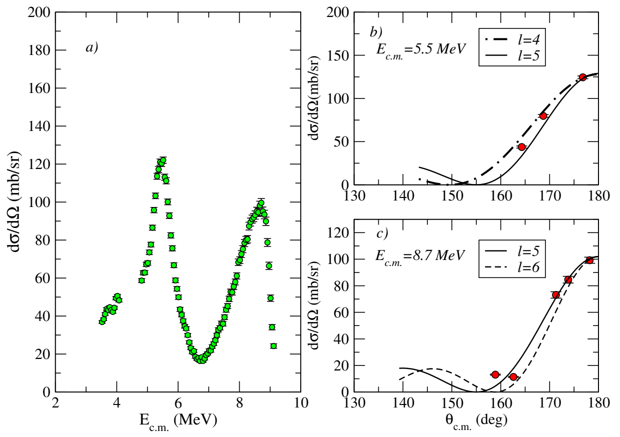


**Figure 2.** a) $^{9}Li+^{4}He$ excitation function in the angular region $175° \leq \theta_{c.m.} \leq 178°$.b) (Symbols) angular distribution at $E_{c.m.}$=5.5 MeV, (dot-dashed line) $\ell$=4, and (full line) $\ell$=5, Legendre polynomials normalised to the experimental cross-section. c) (Symbols) angular distribution at $E_{c.m.}$=8.7, (full line) $\ell$=5, and (dashed line) $\ell$=6, Legendre polynomials normalised to the experimental cross-section.

calculations the potential parameters of the model, such as the radii of the volume and surface term, where deduced from [10]. The potential depths were obtained from reproducing the energies of the resonances. The model predicts cross sections, widths and position of resonances reasonably close to the cross section value and energies of the 5.5 and 8.7 MeV peaks [15] (5 and 9 MeV). This supports the underlying assumption of the model that quasi-molecular states are being formed and those states are originated by the weak absorption at the surface due to the neutron skin present in $^{9}Li$.

## 4 Summary

In this contribution are reported results of low-energy nuclear reaction studies involving one proton-halo and one neutron rich radioactive nuclei. The $^{8}B+^{64}Zn$ elastic scattering investigation at energies around the Coulomb barrier shows that, unlike the neutron-halo case, there are only small effects of coupling to the continuum resulting in a small reduction of the elastic cross section in the nuclear-Coulomb interference peak. The total reaction cross-section is similar to that of ordinary weakly bound nuclei on the same target and not strongly enhanced as for the neutron-halo collisions.

In this contribution is also described the measurement of the $^{9}Li+^{4}He$ elastic scattering excitation function in the energy region 3.5 MeV$\leq E_{c.m.} \leq$9 MeV.

The measured excitation function shows broad resonances. To interpret the data a simplified molecular rotational reaction model was developed. It was found that the model predicts reasonably well the energies and cross section magnitudes of the resonances. These resonances do not seem to be associated to states in the compound nucleus but rather to the formation of quasi-molecular states originated by the weak absorption at the surface due to the neutron-skin present in $^{9}Li$.

## 5 Acknowledgements

This work has been supported by the European Commission Horizon 2020 framework trans-national access program of the EU project ENSAR2 (Grant no. 654002).

## References

[1] A. Sánchez-Benítez, D. Escrig, M. Álvarez, M. Andrés, C. Angulo, M. Borge, J. Cabrera, S. Cherubini, P. Demaret, J. Espino et al., Nucl. Phys. A **803**, 30 (2008)
[2] A. Di Pietro, P. Figuera, F. Amorini, C. Angulo, G. Cardella, S. Cherubini, T. Davinson, D. Leanza, J. Lu, H. Mahmud et al., Phys. Rev. C **69**, 044613 (2004)
[3] M. Cubero, J.P. Fernández-García, M. Rodríguez-Gallardo, L. Acosta, M. Alcorta, M.A.G. Alvarez, M.J.G. Borge, L. Buchmann, C.A. Diget, H.A. Falou et al., Phys. Rev. Lett. **109**, 262701 (2012)
[4] A. Di Pietro, G. Randisi, V. Scuderi, L. Acosta, F. Amorini, M.J.G. Borge, P. Figuera, M. Fisichella, L.M. Fraile, J. Gomez-Camacho et al., Phys. Rev. Lett. **105**, 022701 (2010)
[5] A. Di Pietro, V. Scuderi, A.M. Moro, L. Acosta, F. Amorini, M.J.G. Borge, P. Figuera, M. Fisichella, L.M. Fraile, J. Gomez-Camacho et al., Phys. Rev. C **85**, 054607 (2012)
[6] R. Raabe, J.L. Sida, J.L. Charvet, N. Alamanos, C. Angulo, J.M. Casandjian, S. Courtin, A. Drouart, D.J.C. Durand, P. Figuera et al., Nature **431**, 823 (2004)
[7] J.P. Fernández-García, M. Cubero, M. Rodríguez-Gallardo, L. Acosta, M. Alcorta, M.A.G. Alvarez, M.J.G. Borge, L. Buchmann, C.A. Diget, H.A. Falou et al., Phys. Rev. Lett. **110**, 142701 (2013)
[8] V. Guimarães, J.J. Kolata, D. Peterson, P. Santi, R.H. White-Stevens, S.M. Vincent, F.D. Becchetti, M.Y. Lee, T.W. O'Donnell, D.A. Roberts et al., Phys. Rev. Lett. **84**, 1862 (2000)
[9] M. Mazzocco, N. Keeley, A. Boiano, C. Boiano, M. La Commara, C. Manea, C. Parascandolo, D. Pierroutsakou, C. Signorini, E. Strano et al., Phys. Rev. C **100**, 024602 (2019)
[10] Y. Kanada-En'yo, Y. Kawanami, Y. Taniguchi, M. Kimura, Progress of Theoretical Physics **120**, 917 (2008)
[11] R. Spartà, A. Di Pietro, P. Figuera, O. Tengblad, A. Moro, I. Martel, J. Fernández-García, J. Lei, L. Acosta, M. Borge et al., Physics Letters B **820**, 136477 (2021)
[12] G. Marquínez-Durán, L. Acosta, R. Berjillos, J. Dueñas, J. Labrador, K. Rusek, A. Sánchez-Benítez, I. Martel, Nucl. Instr. and Meth. A **755**, 69 (2014)
[13] E.F. Aguilera, E. Martinez-Quiroz, D. Lizcano, A. Gómez-Camacho, J.J. Kolata, L.O. Lamm, V. Guimarães, R. Lichtenthäler, O. Camargo, F.D. Becchetti et al., Phys. Rev. C **79**, 021601 (2009)

[14] Y.Y. Yang, X. Liu, D.Y. Pang, Phys. Rev. C **94**, 034614 (2016)

[15] A. Di Pietro, A. Shotter, J. Fernández-García, P. Figuera, M. Fisichella, A. Moro, M. Alcorta, M. Borge, T. Davinson, F. Ferrera et al., Physics Letters B **832**, 137256 (2022)

[16] V.Z. Goldberg, G.V. Rogachev, W.H. Trzaska, J.J. Kolata, A. Andreyev, C. Angulo, M.J.G. Borge, S. Cherubini, G. Chubarian, G. Crowley et al., Phys. Rev. C **69**, 024602 (2004)

[17] A. Musumarra, P. Figuera, F. De Luca, A. Di Pietro, P. Finocchiaro, M. Fisichella, M. Lattuada, A. Pakou, M. Pellegriti, G. Randisi et al., Nucl. Instr. Methods A **612**, 399 (2010)

[18] K.W. McVoy, Phys. Rev. C **3**, 1104 (1971)